EMITTANCE TRANSFER IN LINACS

L. Groening, X. Chen, M. Maier, O.K. Kester, GSI, D-64291 Darmstadt, Germany
M. Chung, Ulsan National Institute of Science and Technology, Ulsan 698-798, Republic of Korea

Abstract

Flat beams feature unequal emittances in the horizontal and vertical phase space. Such beams were created successfully in electron machines by applying effective stand-alone solenoid fringe fields in the electron gun. This contribution is an extension of the method to ion beams and on the decoupling capabilities of such a round-to-flat adaptor. The beam line provides a single-knob tool to partition the horizontal and vertical rms emittances, while keeping the product of the two emittances constant as well as the transverse rms Twiss parameters ($\beta_{x,y}$ and $\alpha_{x,y}$) in both planes. This single knob is the solenoid field strength. The successful commissioning of the set-up with beam will be presented as well.

INTRODUCTION

Transformation of a round beam (equal transverse emittances) to a flat beam (different transverse emittances) requires changing the beam eigen-emittances. The eigen-emittances are defined through the beam second moments as

$$\varepsilon_1 = \frac{1}{2}\sqrt{-tr[(CJ)^2] + \sqrt{tr^2[(CJ)^2] - 16det(C)}} \quad (1)$$

$$\varepsilon_2 = \frac{1}{2}\sqrt{-tr[(CJ)^2] - \sqrt{tr^2[(CJ)^2] - 16det(C)}}, \quad (2)$$

where

$$C = \begin{bmatrix} \langle xx\rangle & \langle xx'\rangle & \langle xy\rangle & \langle xy'\rangle \\ \langle x'x\rangle & \langle x'x'\rangle & \langle x'y\rangle & \langle x'y'\rangle \\ \langle yx\rangle & \langle yx'\rangle & \langle yy\rangle & \langle yy'\rangle \\ \langle y'x\rangle & \langle y'x'\rangle & \langle y'y\rangle & \langle y'y'\rangle \end{bmatrix} \quad (3)$$

and

$$J = \begin{bmatrix} 0 & 1 & 0 & 0 \\ -1 & 0 & 0 & 0 \\ 0 & 0 & 0 & 1 \\ 0 & 0 & -1 & 0 \end{bmatrix}. \quad (4)$$

Linear transport elements as drifts, quadrupoles, dipoles, and rf-gaps do not change neither the beam rms emittances nor the eigen-emittances. Solenoids, skew quadrupoles, and -dipoles change the rms emittances through x-y coupling. But they do not change the eigen-emittances. This is often expressed by the simplecticity criterion for the transport matrix M representing the transport element [1]

$$M^T J M = J. \quad (5)$$

A matrix M satisfying the above criterion, is called symplectic and the eigen-emittances of a beam being transported by M remain constant. Beam particle coordinates are expressed by displacements x and y in space and by the respective derivatives x' and y' w.r.t. the longitudinal coordinate s. The matrix of a solenoid fringe field reads as

$$M_F = \begin{bmatrix} 1 & 0 & 0 & 0 \\ 0 & 1 & k & 0 \\ 0 & 0 & 1 & 0 \\ -k & 0 & 0 & 1 \end{bmatrix} \quad (6)$$

with $k = \frac{B}{2(B\rho)}$. B is the solenoid on-axis magnetic field strength and $B\rho$ is the beam rigidity. M_F does not satisfy Equ. 5 and changes the eigen-emittances. However, it leaves constant the 4d rms emittance defined as the square root of the determinant of C from Equ. 3.

Stand-alone fringe fields do not exist since magnetic field lines are closed. Effective stand-alone fringe fields act on the beam if the beam charge state is changed in between the fringes of the same solenoid. This is the case for rf-guns [2,3] (free electron creation inside solenoid), extraction from an Electron-Cyclotron-Resonance ion source [4] (ionisation inside the solenoid), and for charge state stripping inside a solenoid [5]. Further discussion of symplecticity of fringes shall be avoided here and we refer to [6] instead. We just point out that changing the ion beam charge state is equivalent to cancelling the stripped-off electrons from the system. This cancellation is a non-symplectic action and conservation of the eigen-emittances within the remaining subsystem cannot by assumed in general.

In this report we assume that an effective fringe field (Equ. 6) coupled an initially round & decoupled beam. The second moments matrix of this beam at the entrance to that fringe is given by

$$C_1' = \begin{bmatrix} \varepsilon\beta & 0 & 0 & 0 \\ 0 & \frac{\varepsilon}{\beta} & 0 & 0 \\ 0 & 0 & \varepsilon\beta & 0 \\ 0 & 0 & 0 & \frac{\varepsilon}{\beta} \end{bmatrix}, \quad (7)$$

where ε is the rms emittance in both transverse planes and β is the rms beta function.

The report is organized in the following: in the first section we repeat parts of references [7] and [8], i.e. decoupling of the beam using a generic decoupling beam line. The subsequent section treats the extension of the generic case to any decoupling beam line. Finally, we report on successful experimental demonstration of one-knob emittance transfer.

DE-COUPLING FOR THE GENERIC CASE

The beam second moment matrix after passing the fringe field of Equ. 6 is

$$C_2' = M_F C_1' M_F^T = \begin{bmatrix} \varepsilon_n R_n & -k\varepsilon_n\beta_n J_n \\ k\varepsilon_n\beta_n J_n & \varepsilon_n R_n \end{bmatrix}, \quad (8)$$

ISBN 978-3-95450-173-1

where

$$\varepsilon_n = \sqrt{\varepsilon\beta(\frac{\varepsilon}{\beta} + k^2\varepsilon\beta)}, \quad \beta_n = \frac{\beta\varepsilon}{\varepsilon_n}, \tag{9}$$

introducing the 2×2 sub-matrices R_n and J_n as

$$R_n = \begin{bmatrix} \beta_n & 0 \\ 0 & \frac{1}{\beta_n} \end{bmatrix}, \quad J_n = \begin{bmatrix} 0 & 1 \\ -1 & 0 \end{bmatrix}. \tag{10}$$

Inter-plane coupling is created and the rms emittances and eigen-emittances after the fringe read

$$\varepsilon_{x,y} = \varepsilon_n, \quad \varepsilon_{1,2} = \varepsilon_n(1 \mp k\beta_n). \tag{11}$$

The parameter t is introduced to quantify the interplane coupling. If t defined as

$$t = \frac{\varepsilon_x\varepsilon_y}{\varepsilon_1\varepsilon_2} - 1 \geq 0 \tag{12}$$

is equal to zero, there are no inter-plane correlations and the beam is fully decoupled.

Obtaining this result we neglected the finite solenoid length, i.e. its central longitudinal field. Tracking simulations using 3D-field maps of finite solenoids confirmed that this omission is justified [9].

As shown for instance by Kim [7] the beam represented by Equ. 8 is decoupled through a beam line formed by an identity matrix in the x-direction and an additional 90° phase advance in y-direction

$$R_q = \begin{bmatrix} I_n & O_n \\ O_n & T_n \end{bmatrix}. \tag{13}$$

Here the 2×2 sub-matrices O_n, T_n and I_n are defined as

$$O_n = \begin{bmatrix} 0 & 0 \\ 0 & 0 \end{bmatrix}, \quad T_n = \begin{bmatrix} 0 & u \\ -\frac{1}{u} & 0 \end{bmatrix}, \quad I_n = \begin{bmatrix} 1 & 0 \\ 0 & 1 \end{bmatrix}. \tag{14}$$

If the quadrupoles are tilted by 45° the 4×4 transfer matrix can be written as

$$\overline{R} = R_r R_q R_r^T = \frac{1}{2}\begin{bmatrix} T_{n+} & T_{n-} \\ T_{n-} & T_{n+} \end{bmatrix}, \tag{15}$$

where

$$R_r = \frac{1}{\sqrt{2}}\begin{bmatrix} I_n & I_n \\ -I_n & I_n \end{bmatrix}, \quad T_{n\pm} = T_n \pm I_n. \tag{16}$$

The beam matrix $C_3^{'}$ after the decoupling section is

$$C_3^{'} = \overline{R}C_2^{'}\overline{R}^T = \begin{bmatrix} \eta_+\Gamma_{n+} & \zeta\Gamma_{n-} \\ \zeta\Gamma_{n-} & \eta_-\Gamma_{n+} \end{bmatrix}, \tag{17}$$

and the 2×2 sub-matrices $\Gamma_{n\pm}$ are defined through

$$\Gamma_{n\pm} = \begin{bmatrix} u & 0 \\ 0 & \pm\frac{1}{u} \end{bmatrix}, \tag{18}$$

with

$$\eta_\pm = \frac{\varepsilon_n}{2}(\frac{\beta_n}{u} + \frac{u}{\beta_n} \mp 2k\beta_n) \tag{19}$$

and

$$\zeta = \frac{\varepsilon_n}{2}(-\frac{\beta_n}{u} + \frac{u}{\beta_n}). \tag{20}$$

Assuming that this beam matrix is diagonal, its x-y component vanishes

$$\zeta\Gamma_{n-} = O_n \tag{21}$$

solved by

$$u = \pm\beta_n, \tag{22}$$

where the positive sign indicates that ε_x is made equal to ε_1 by decoupling and the negative sign means that ε_y is made equal to ε_1. We calculate the final rms emittances obtaining

$$\varepsilon_{x,y} = |\varepsilon_n(1 \mp k\beta_n)|. \tag{23}$$

For a given effective solenoid fringe field strength k_0, the corresponding quadrupole gradients may be determined using a numerical routine, such that finally the rms emittances are equal to the eigen-emittances. If these optimized gradients are applied to remove interplane correlations produced by a different fringe strength k_1, the resulting rms emittances and eigen-emittances at the exit of the decoupling section are calculated as

$$\varepsilon_{x,y} = \frac{\varepsilon_n(k_1)}{2}\left|\frac{\beta_n(k_1)}{\beta_n(k_0)} + \frac{\beta_n(k_0)}{\beta_n(k_1)} \mp 2k_1\beta_n(k_1)\right| \tag{24}$$

and

$$\varepsilon_{1,2} = \varepsilon_n(k_1)|1 \mp k_1\beta_n(k_1)| \tag{25}$$

with the parameter

$$t = \frac{\varepsilon^2\beta^2}{\frac{\varepsilon}{\beta}(\frac{\varepsilon}{\beta} + k_0^2\varepsilon\beta)}\frac{(k_1^2 - k_0^2)^2}{4}. \tag{26}$$

In the same way the rms Twiss parameters of a beam coupled by k_1 but decoupled by $\overline{R}(k_0)$ are found from Equ. (17) as

$$\tilde{\alpha}_x = \tilde{\alpha}_y = 0, \quad \tilde{\beta}_x = \tilde{\beta}_y = \beta_n(k_0), \tag{27}$$

showing that the rms Twiss parameters after decoupling do not depend on the coupling solenoid fringe strength k_1 if the decoupling section was set assuming a coupling strength k_0. We stress the very convenient feature of the generic decoupling line $\overline{R}$: once a decoupling set of gradients has been found for the fringe field strength k_o, these gradients will practically decouple also beams coupled by a different strength $|k_1| \leq |k_0|$. This is shown in Fig. 1, which was originally presented in [8]. Moreover, the Twiss parameters β and α at the exit of the generic beam line $\overline{R}$ do not depend on the fringe strength. These two features enormously facilitate the design and operation of such a round-to-flat adapter.

ISBN 978-3-95450-173-1

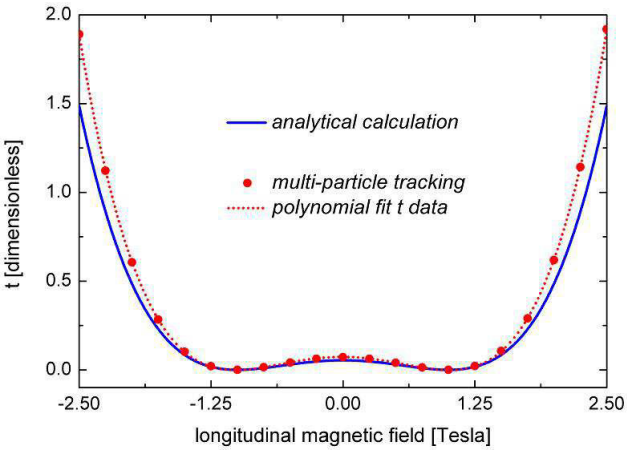

Figure 1: The coupling parameter t at the exit of the generic beam line $\overline{R}$ as a function of the solenoid field causing the fringe field strength k_1 (blue line). The figure is taken from [8] and k_0 corresponds to 1.0 T. The dependency is described by Equ. 26.

DECOUPLING FOR THE GENERAL CASE

In the previous section we derived the following ensemble $\mathcal{P}$ of properties of the generic decoupling line $\overline{R}$ of Equ. 15:

- t at the exit scales as $(k_1^2 - k_0^2)^2$, where k_o is the assumed fringe strength and k_1 is the strength actually applied for the coupling. $t << 1$ holds over a wide range of k_1 (Equ. 26 and Fig. 1 with $B \sim k_1$).
- the exit Twiss parameters $\beta_x, \alpha_x, \beta_y, \alpha_y$ do not depend on the actual fringe strength k_1 (Equ. 27).
- the only quantity considerably changed through the fringe strength is the transverse rms emittance partitioning $\varepsilon_x/\varepsilon_y$ (Equ. 24).

It must be stressed that these properties hold for both signs in Equ. 22. However, [8] found by various tracking simulations with TRACK [10] as well as by applying the matrix formalism, that $\mathcal{P}$ seems to hold for any beam line M_D that provides decoupling of a round beam previously coupled through a stand-alone solenoid fringe field. This feature was not understood in [8].

Instead it can be understood through the procedure being illustrated in Fig. 2. Suppose there is any arbitrary beam line M_D that provides decoupling. This beam line includes x-y coupling linear elements. We prolong M_D by a beam line represented by the matrix

$$A = \begin{bmatrix} A_x & O_n \\ O_n & A_y \end{bmatrix} \qquad (28)$$

with the 2×2 sub-matrices A_x and A_y. A must not include any x-y coupling element.

The resulting total beam line is the product AM_D. We choose for the non-coupling line $A = \overline{R}M_D^{-1}$ such that $\overline{R} = AM_D$.

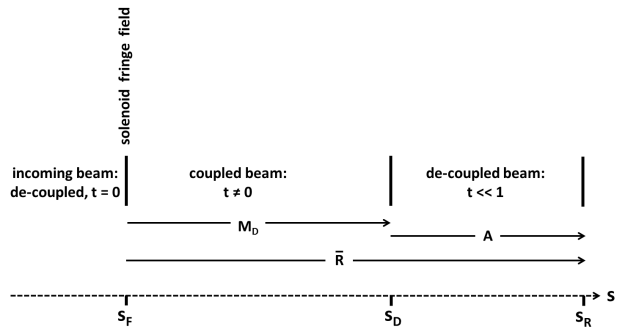

Figure 2: Extension of the decoupling features of the generic beam line $\overline{R}$ to any decoupling beam line M_D. S_F denotes the location of the initially coupling stand-alone solenoid fringe field. The arbitrary decoupling beam line M_D ends at S_D, and the generic beam line $\overline{R}$ ends at S_R. The beam line A does not include any x-y coupling element.

Care is to be taken in choosing the right sign at Equ. 22 in the construction of $\overline{R}$. This is to assure that both, M_D and $\overline{R}$, reduce ε_x to the same of the two eigen-emittances. Choosing the wrong sign, A gets an emittance exchange beam line that includes coupling elements. As shown above, at the exit of $\overline{R}$ the properties $\mathcal{P}$ hold. From the exit of $\overline{R}$ the Twiss parameters ε, β, and α (in both planes) are transported backwards to S_D by applying A^{-1} being aware that α and β do not depend from the fringe strength. As A does not include any x-y coupling element, neither does A^{-1}. Accordingly, the back-transformed Twiss parameters at S_D also do not depend on the fringe strength. The same way the invariance of the Twiss parameters w.r.t. the fringe strength is kept through the back-transportation by A^{-1}, the weak dependence of $t(k_1)$ is back-transported & preserved through A^{-1}. Since A^{-1} is non-coupling, it preserves t. In other words, the properties $\mathcal{P}$ at the exit of $\overline{R}$ are preserved during back-transportation by A^{-1}. As a consequence the properties $\mathcal{P}$ hold also at the exit of the arbitrarily chosen decoupling beam line M_D.

EXPERIMENTAL DEMONSTRATION

The EMitance Transfer EXperiment (EMTEX) was installed [11] last year along the transfer channel from GSI's UNIversal Linear ACcelerator (UNILAC) to the synchrotron. Figure 3 shows the set-up starting with two doublets to match

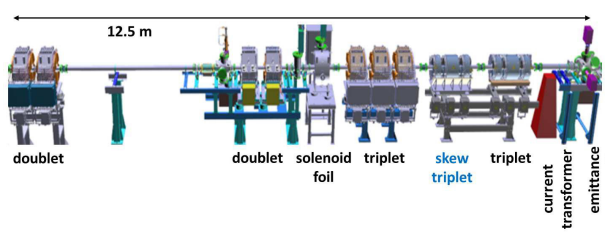

Figure 3: Beam line of EMTEX (Emittance Transfer Experiment).

ISBN 978-3-95450-173-1

the beam to the entrance of the short solenoid, which provides inter-plane coupling. The foil can be moved into the solenoid center. Stripping in the foil causes the entrance and exit fringe fields to act differently on the beam. Together with the fact that the solenoid is sufficiently short, this set-up provides for an effective stand-alone solenoid fringe field modelled through Eq. 6. After the solenoid the coupled beam is matched by a triplet to the skew triplet that provides decoupling. Another regular triplet re-matches the beam for further transport. It is followed by a slit-grid beam emittance meter which allows for measuring the phase space distribution in the horizontal and vertical planes.

For the experiment a low intensity beam of $^{14}N^{3+}$ at 11.4 MeV/u was used. First, all EMTEX magnets were turned off and the stripping foil was removed from the solenoid. Full beam transmission was assured by using beam current transformes installed in front of and behind EMTEX. In order to assure that the beam in front of EMTEX does not exhibit already some inter-plane correlations, its image was observed using a fluorescence screen. The image was observed under variation of a quadrupole being installed in front of the screen. The quadrupole strength was varied to deliver a large spectrum of beam spot aspect ratios. Considerable inter-plane correlations would have manifested through tilted beam images. As only upright images were observed, it was assumed that no inter-plane correlations are present at the entrance to EMTEX.

In the following step, beam emittances were measured in both planes at the exit of EMTEX. The obtained Twiss parameters together with the settings of the first two doublets were used to determine the beam Twiss parameters at the entrance to the first doublet of EMTEX. A horizontal (vertical) rms emittance of 1.04 (0.82) mm mrad was measured. Both doublets were set to provide a small beam with double waist at the location of the foil. The foil (carbon, 200 μg/cm^2, 30 mm in diameter) was moved into the solenoid. The measured beam current transmission increased by a factor of 2.3 as expected from charge state stripping of the beam from 3+ to 7+. Beam phase probes behind EMTEX were used to detect eventual beam energy loss induced by the foil. Within the resolution of the probes we assume that energy loss is close to the calculated value of 0.026 MeV/u from the ATIMA code [12]. The same code was used to calculate the mean angular scattering of 0.474 mrad per plane. After determining all required input parameters the solenoid field was set to 0.9 T. Applying a numerical routine the three triplets behind the solenoid were set to decouple the beam and to provide for a beam with small vertical and large horizontal emittance together with full transmission through the entire set-up. These gradients were set and full beam transmission was preserved. Just very few steering was needed to re-center the beam in the emittance meter. This was required due to slight misalignment of the solenoid axis w.r.t. the beam axis. For the setting mentioned above both transverse emittances were measured. Afterwards the solenoid field was reduced stepwise to 0 T. The solenoid field B_i was set by following the remanence-mitigating path $B_{i-1} \rightarrow B_{max} \rightarrow 0\,T \rightarrow B_i$. All quadrupole gradients were kept constant. For each solenoid setting full transmission was preserved and both emittances were measured.

Figure 4 plots the measured rms emittances behind EMTEX as functions of the solenoid field strength. With increasing solenoid field the vertical emittance decreases while the horizontal increases. The product of the two emittances remains constant within the precision of the measurement. This behaviour is in full agreement to theoretical predictions from [8] and to tracking simulations with TRACK [10] using magnetic field maps. It is also in agreement with calculations that apply the recently developed 4d-envelope model for coupled lattices [13–16]. The observed emittance separation under variation of the solenoid field only, confirms that EMTEX is an one-knob tool for adjustable emittance partitioning.

Figure 5 displays measured phase space distributions as functions of the solenoid field strength. It demonstrates that the shapes of the occupied areas in phase space and espe-

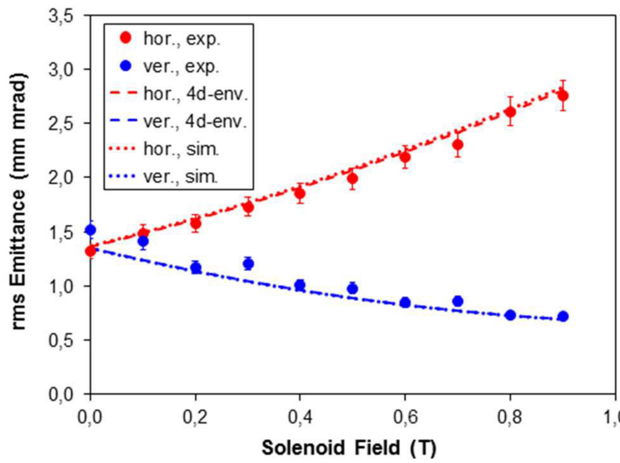

Figure 4: Vertical (blue) and horizontal (red) rms emittances at the exit of the EMTEX beam line as functions of the solenoid field strength. All other settings were kept constant. Shown are results from measurements (dots), from application of the 4d-envelope model for coupled lattices (dashed), and from tracking simulations (dotted).

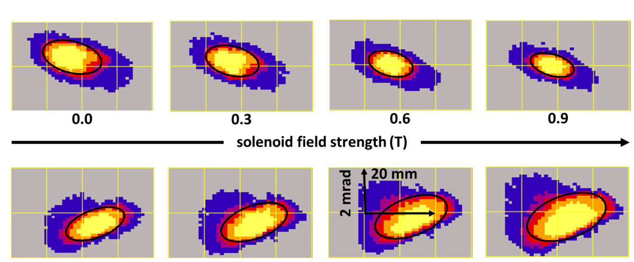

Figure 5: Vertical (upper) and horizontal (lower) phase space distributions measured at the exit of the EMTEX beam line as functions of the solenoid field strength. All other settings were kept constant. Black ellipses indicate the 4×rms ellipses.

ISBN 978-3-95450-173-1

cially the shapes of the corresponding 4×rms ellipses do not depend on the solenoid field strength within the resolution of the measurement. Also this experimental result is in full agreement to the observation from simulations reported in [8] and to the properties of EMTEX derived previously. These references assume a beam with exactly equal transverse emittances at the entrance of EMTEX. The beam emittances in the experiment differed by 23% from each other. However, the quasi-invariance of the final ellipse shapes is in excellent agreement with the 4d-envelope model and with tracking simulations also for the presented experiment. Accordingly, the experimental data also confirm that EMTEX is a one-knob emittance partitioning tool that preserves the beam envelope functions β and α at its exit, if the initial beam emittances are similar. This feature makes it obsolete to re-match the envelopes as a function of the desired emittance partitioning once the partitioning is completed.

The emittance partitioning is given by the solenoid field strength. As shown in [8], inversion of the solenoid field swaps the behaviours of the emittances displayed in Fig. 4, i.e. for negative solenoid field strengths the vertical emittance increases and the horizontal one decreases with the field strength. This could not be tested experimentally, since the solenoid power converter was uni-polar. However, inversion of the solenoid field strength is fully equivalent to inversion of the skew quadrupole gradients, while keeping all other gradients and the solenoid field constant. Inversion of the skew gradients corresponds to rotation of the skew quadrupoles by 90° , i.e. to swapping the transverse planes. Accordingly, the sense of emittance partitioning is inverted for inverted skew gradients. This was verified experimentally as shown in Fig. 6. Also for inverted skew quadrupole gradients, preservation of the orientations and shapes of the measured phase space distributions was observed. Just the sizes of the corresponding 4×rms ellipses changed with the solenoid field strength. For inverted skew quadrupoles the agreement to theory and to simulations is still good but slightly worse than for the case shown in Fig. 4. Additionally, for a given solenoid field value the horizontal emittance values shown in Fig. 6 are not exactly equal to the vertical emittance values shown in Fig. 4. According to theory they should be equal. However, the differences are very small. We attribute them to remanence effects in the solenoid and in the bi-polar skew triplets.

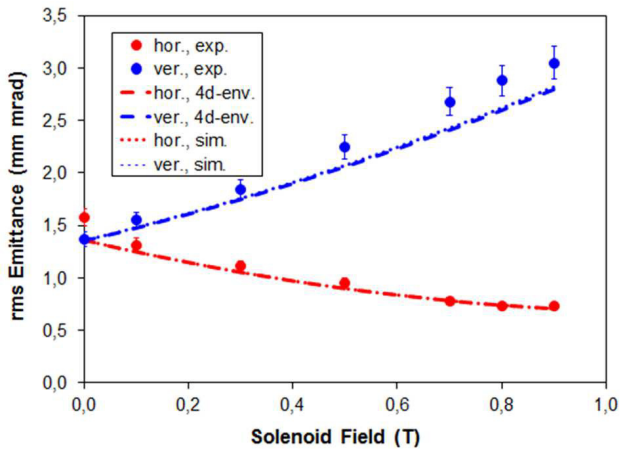

Figure 6: Vertical (blue) and horizontal (red) rms emittances at the exit of the EMTEX beam line as functions of the solenoid field strength. All other settings were kept constant. Shown are results from measurements (dots), from application of the 4d-envelope model for coupled lattices (dashed), and from tracking simulations (dotted). W.r.t. Fig. 4 the gradients of the skew quadrupoles are inverted.

REFERENCES

[1] A.J. Dragt, Phys. Rev. A **45**, 4 (1992).

[2] R. Brinkmann, Y. Derbenev, and K. Flöttmann, Phys. Rev. ST Accel. Beams **4**, 053501 (2001).

[3] D. Edwards, H. Edwards, N. Holtkamp, S. Nagaitsev, J. Santucci, R. Brinkmann, K. Desler, K. Flöttmann, I. Bohnet, and M. Ferrario, in *Proceedings of the XX Linear Accelerator Conference, Monterey, CA,* edited by A. Chao, e000842 (2000).

[4] P. Bertrand, J.P. Biarrotte, and D. Uriot, in Proceedings of the 10th European Accelerator Conference, Edinburgh, Scotland, edited by J. Poole and C. Petit-Jean-Genaz (Institute of Physics, Edinburgh, Scotland, 2006).

[5] L. Groening, Phys. Rev. ST Accel. Beams **14**, 064201 (2011).

[6] C. Baumgarten, Nucl. Instrum. & Methods **A 735**, p. 546 (2014).

[7] K.-J. Kim, Phys. Rev. ST Accel. Beams **6**, 104002 (2003).

[8] C. Xiao, L. Groening, O. Kester, H. Leibrock, M. Maier, and C. Mühle, Phys. Rev. ST Accel. Beams **16**, 044201 (2013).

[9] C. Xiao, L. Groening, and O. Kester, Proceedings of the 52nd ICFA Advanced Beam Dynamics Workshop, Beijing, PR China, edited by J. Wang (Institute of High Energy Physics, Beijing, PR China, 2012).

[10] P. Ostroumov, TRACK version-37, user manual, http://www.phy.anl.gov/atlas/TRACK/

[11] M. Maier, L. Groening, C. Mühle, I. Pschorn, P. Rottländer, C. Will, C. Xiao, and M. Chung, Proceedings of the 5th International Particle Acceleratore Conference, Dresden, Germany, edited by C. Petit-Jean-Genaz (CERN, Geneva, Switzerland, 2014).

[12] http://web-docs.gsi.de/weick/atima/

[13] Hong Qin, Moses Chung, and Ronald C. Davidson, Phys. Rev. Lett. **103**, 224802 (2009).

[14] Hong Qin, Ronald C. Davidson, Moses Chung, and Joshua W. Burby, Phys. Rev. Lett. 111, 104801 (2013).

[15] Hong Qin, Ronald C. Davidson, Joshua W. Burby, and Moses Chung, Phys. Rev. ST Accel. Beams **17**, 044001 (2014).

[16] Moses Chung, Hong Qin, Lars Groening, Ronald C. Davidson, and C. Xiao, *Beam Envelope Calculations in General Linear Coupled Lattices*, submitted to Phys. Plasmas.

ISBN 978-3-95450-173-1